ChemPubSoc Europe

DOI: 10.1002/celc.201700326

CHEMELECTROCHEM Articles

PtSn Electrocatalyst Supported on MWCNT-COOH: Investigating the Ethanol Oxidation Reaction

Luanna Silveira Parreira,[b] Júlio César Martins Silva,[a] Fábio Ruiz Simões,[c] Marco Aurélio Liutheviciene Cordeiro,[d] Roseli Hiromi Sato,[a] Edson Roberto Leite,[c] and Mauro Coelho dos Santos*[a]

Pt_3Sn_2 (a:a) electrocatalysts with 20% metal loading on multi-walled carbon nanotube supports functionalized with carboxylic acid groups (MWCNT-COOH) were prepared for studies on the ethanol oxidation reaction (EOR). Preparing and anchoring of the metallic nanoparticles increased the hydrophilicity of MWCNT-COOH and decreased its surface roughness to a value close to that of the commercial electrocatalyst Pt_3Sn_1/C E-TEK. Pt_3Sn_2/MWCNT-COOH consisted of 32% Pt_3Sn alloy with a lattice parameter of 0.3979 nm. The mean particle size of 3.85 ± 1.17 nm was measured by high-resolution transmission electron microscopy (HRTEM). The onset oxidation potential obtained for the EOR (in the cyclic voltammetry experiments) using Pt_3Sn_2/MWCNT-COOH was the lowest (0.21 V vs. reversible hydrogen electrode (RHE)), with a normalized current peak of 250 mA mg_{Pt}^{-1}. The highest normalized current in the chronoamperometric measurements for the EOR after 1800 seconds at 0.5 V (RHE) was 16 mA mg_{Pt}^{-1}, whereas for Pt_3Sn_1/C E-TEK it was 10 mA mg_{Pt}^{-1}. FTIR-ATR in situ analysis showed that the Pt_3Sn_2/MWCNT-COOH electrocatalyst favoured acetaldehyde production at lower potentials and CO_2 production at potentials greater than 0.5 V. In addition, the presence of oxygenated functional groups on the nanotube surfaces together with the anchoring of Pt and SnO_2 formation contributed to the oxidation of ethanol to CO_2 (bifunctional mechanism), enhancing the electrocatalytic activity of the material compared to commercial Pt_3Sn_1/C E-TEK.

1. Introduction

Society is currently characterized by fast economic and social growth, with increasing energy consumption and greenhouse gas emissions that are mainly derived from fossil fuels. These resources can be depleted, and their combustion may cause climate change. Thus, the search for clean and renewable energy sources has intensified. In this context, fuel cells have been proposed as an alternative for obtaining energy in a clean and renewable way.

Fuel cells[1,2] spontaneously transform stored chemical energy from electrochemical reactions into electrical energy. Ethanol has gained prominence in low-temperature fuel cells because it can be produced from biomass and it has a lower toxicity and higher energy density (8.01 kWh kg^{-1} vs. 6.09 kWh kg^{-1}) than methanol. However, the electrochemical oxidation of ethanol is more complex, involving the release of 12 electrons and the cleavage of a C–C bond. In addition, the main products beyond two-carbon intermediates include adsorbed CO, CH_3CHO, CH_3COOH and CO_2.

To promote the electrochemical oxidation of ethanol, one of the best electrocatalyts is PtSn/C, which is commonly used at an atomic ratio of 3:1. PtSn/C has shown promising results for ethanol oxidation.[3–7] However, further discussion is required regarding the best methods for the preparation, alloying and oxide formation in the electrocatalysts, in addition to other factors that define electrocatalytic activity.

Souza et al.[8] suggested that the activity of the Pt_3Sn/C electrocatalyst results from an electronic effect in the alloy phase, where Sn changes the electron density of the "5d" Pt band, weakening the adsorption of the reaction intermediates (such as CO), facilitating the release of metal active sites, and increasing the electrocatalytic activity of the material. Jiang et al.[9] showed that the oxidation state of Sn affects the influence of Sn on Pt and the electrode stability because higher oxidation states promote the electrochemical oxidation of ethanol by bifunctional mechanisms that depend on the electrocatalyst preparation method. Zhu et al.[10] prepared three

[a] Dr. J. C. M. Silva, Dr. R. H. Sato, Dr. M. C. dos Santos
Laboratório de Eletroquímica e Materiais Nanoestruturados
Centro de Ciências Naturais e Humanas
Universidade Federal do ABC
Rua Santa Adélia 166
CEP 09.210-170, Santo André, SP (Brazil)
Fax: 55 (11) 4996-0090
E-mail: mauro.santos@ufabc.edu.br
[b] Dr. L. S. Parreira
Departmento de Química Fundamental
Instituto de Química
Universida de de São Paulo
Av. Prof. Lineu Prestes 748, CEP 05508-000, São Paulo, SP (Brazil)
[c] Dr. F. R. Simões, Dr. E. R. Leite
Departamento de Ciências do Mar
Universidade Federal de São Paulo
Campus da Baixada Santista
Av. Alm. Saldanha da Gama 89
CEP 11030-400, Ponta da Praia – Santos, SP (Brazil)
[d] Dr. M. A. L. Cordeiro
Departamento de Química
Universidade Federal de São Carlos
Rodovia Washington Luís km 235
CEP 13.565-905, São Carlos, SP (Brazil)

Supporting information for this article is available on the WWW under https://doi.org/10.1002/celc.201700326

PtSn electrocatalysts at an atomic ratio of 3:1 using different methods to obtain varying alloy degrees. The materials with higher alloy degrees promoted the dehydrogenation of ethanol to acetaldehyde and CO_2 via an electronic effect, increasing the electrocatalyst activity. Godoi and colleagues[11] studied the ethanol oxidation reaction using PtSn/C and concluded that the presence of oxides and alloys in the electrocatalyst strongly influences the electrocatalytic activity of the material, indicating that the alloy phase tends to intensify this property. This was recently corroborated in the work of Asgardi et al.,[7] in which the addition of Sn and the content of the Pt_3Sn_1 crystallite phase strongly improved the platinum activity towards carbon monoxide and ethanol electrooxidation.

Another important parameter for the ethanol oxidation reaction is the support of the electrocatalyst. The most promising electrocatalysts for the oxidation of small organic molecules are supported on high-surface-area carbon, which is porous and has good conductivity but only acts as a support and as an appropriate medium for the diffusion of gases in gas diffusion electrodes.[12] In contrast, several studies[13–17] have suggested that carbon nanotubes (CNTs) and graphene nanoribbons (GNRs),[14] when used as supports, increase the electrocatalytic activity of the materials for the oxidation of small organic molecules, such as ethanol and methanol in acidic and alkaline media. Consequently, these materials have good mechanical properties, an electrical conductivity that is as good as or better than that of graphitic carbon, and greater resistance to corrosion phenomena due to the graphitic structure, enabling their use as a support.

Carbon nanotubes are chemically inert, which prevents metallic nanoparticle deposition. Thus, functionalization methods are necessary to create defects and to introduce functional groups to act as anchorage sites, favouring higher metal loading and increasing the surface hydrophilicity of the nanotube surface.[18,19] Thereby, functionalization by both oxygen and carboxyl groups has been employed.[20]

In this context, Sieben and Duarte[15] studied Pt and PtSn supported on oxidized carbon nanotubes prepared using multiple potentiostatic pulses. The authors obtained particles that formed 4–6 nm clusters along the substrate. The formation of solid solutions was observed when the Sn concentration was between 10 and 40%. For the ethanol oxidation reaction at a potential of less than 0.5 V, the metal catalyst with 40% Sn showed the highest electrocatalytic activity. However, above 0.5 V, the alloy with 25% Sn showed better results. The different behaviour resulted from the synergistic effect of Sn, which provides oxygen species that facilitate the oxidation of ethanol, changes the electronic structure of the Pt atoms by weakening the adsorption of CO and other intermediates, and alters the particle size to maximize the electrocatalytic effect. Furthermore, increasing the Pt lattice parameter and the presence of grain boundaries can improve the adsorption of alcohols and favour C–C bond breakage.

Chu et al.[16] developed ternary electrocatalysts with different molar compositions that were supported on CNTs prepared by chemical reduction. The Pt_3SnIn/CNTs 3:01:01 (atomic ratio) electrocatalyst had better activity for ethanol oxidation than materials with the same compositions that were supported on amorphous carbon and binary Pt_3Sn/CNTs electrocatalysts. However, the authors argued that this activity was due to factors such as the three-dimensionality and high specific surface area of the CNTs and the presence of small and highly dispersed particles that contributed to the significant increase in the number of active sites. Furthermore, the presence of active groups, such as carboxylic acid and hydroxide (–COOH and –OH), in the edges and walls of the functionalized CNTs following acid treatment and the large number of species containing oxygen assist the ethanol oxidation process.

Therefore, this work aims to study a Pt_3Sn_2/MWCNT-COOH electrocatalyst prepared by the polymeric precursor method at a metal load of 20% (w:w) on the support for the ethanol oxidation reaction. Additionally, observing its physico-chemical properties and the electrocatalytic activity related to the studied materials in previous work[21,22] obtained from the same prepared method conditions but a different support. The presence of oxygen and carboxylate functional groups was analysed by FTIR in transmittance mode, and the wettability was analysed by contact angle measurements. The phases and lattice parameters were measured by X-ray diffraction (XRD), and the dispersion and average particle sizes were measured by HRTEM. The chemical composition was evaluated by energy dispersive spectroscopy (EDS). Electrochemical techniques, such as cyclic voltammetry and chronoamperometry, were used to measure the electrocatalytic activities of the materials, and Pt_3Sn_1/C E-TEK commercial electrocatalyst was used as reference material for ethanol oxidation reaction. In situ infrared spectroscopy (FTIR) was used to identify the products that were formed in the ethanol oxidation reaction, which is one of the main issues discussed in this paper because there are no papers in the literature, to the best of our knowledge, concerning this issue using the same preparation method with multiwalled carbon nanotubes as the support.

2. Materials and Methods

2.1. Preparation of the Electrocatalyst

The electrocatalyst nanoparticles were prepared using the polymeric precursor method developed by Souza et al.[8] The precursor resin was formed by dissolving citric acid in ethylene glycol at 60 °C, followed by the addition of a metal solution ($H_2PtCl_6.7H_2O$ and $SnCl_2 \cdot 2H_2O$ from Aldrich®) to obtain an electrocatalyst with a metal mass ratio of 3:1. The metal/citric acid/ethylene glycol molar ratio was 1:50:200. The resin was added to COOH-functionalized multiwalled carbon nanotubes (MWCNT-COOH) (Cheaptubes®, Cambridgeport, USA) to obtain a catalyst with a metal loading of 20% (w/w) on the carbon support. The mixture was homogenized in an ultrasonic bath and thermally treated using a vacuum muffle furnace EDG FCVE II under an N_2 atmosphere. The heating rate was 5 °C min^{-1}. In a first step the material was maintained under 110 °C during 10 minutes for water evaporation. Then, the temperature is

elevated to 400 °C (5 °C min^{-1}) and kept during 2 hours producing an electrocatalyst powder.

2.2. Physicochemical Characterization

The functional groups on the MWCNT-COOH surface were measured using a Shimadzu IR Prestige21 FTIR spectrometer. The spectra were obtained from 400 to 4000 cm^{-1} with a resolution of 4 cm^{-1}.

The wettability of the MWCNT-COOH, Pt_3Sn_2/MWCNT-COOH and Pt_3Sn_1/C E-TEK electrocatalyst materials were analysed by contact angle (θ) measurements using a PixelLINK® Camera and Digidrop software. Twenty microlitres of each sample suspension was pipetted onto a glassy carbon plate and was dried by an N_2 flow. One drop (5 μL) of water was deposited on the film and monitored for 10 minutes. For each material, the measurements were performed in triplicate.

X-ray diffraction (XRD) was performed using a Bruker Focus diffractometer with a CuKα radiation source that was operated in continuous scan mode (2° min^{-1}) from 20° to 80° (2θ degrees) to determine the crystalline phases and to estimate the mean crystallite size.

Atomic force microscopy (AFM) imaging of materials was performed using an Agilent Technologies 5500 AFM/SPM microscope in contact mode with a Nanosensors™ PPP-CONT probe (NanoWorld; Cont-50, Point Probe® series) with a force constant of 3.4×10^{-2} N/m. At least 3 different areas of the samples were analysed. The image processing and roughness analysis was conducted using Gwyddion software (http://gwyddion.net/download.php).

High-resolution transmission electron microscopy (HRTEM) analyses were performed using a high-resolution JEOL microscope operating at 300 kV to observe the morphology of the particles and to measure their sizes. All the samples for the HRTEM analysis were prepared by ultrasonically dispersing the catalyst particles in a formaldehyde solution. Drops of the suspension were deposited onto a standard Cu grid and were covered with a carbon film. The average particle size was determined using the Image J software package, and more than 250 different particles were analysed.

Energy dispersive spectroscopy (EDS) using a scanning electron microscope (FESEM JSM – 6701F JEOL) operating at 20 kV was used to measure the chemical composition of the Pt_3Sn_2/MWCNT-COOH electrocatalysts.

2.3. Electrochemical Activity Measurements

The electrochemical experiments were performed using an Autolab model PGSTAT 302 N potentiostat/galvanostat connected to a three-electrode electrochemical cell consisting of one glassy carbon (GC) compartment with a geometric area of 0.071 cm^2, which was used as a support for the working electrodes. A Pt sheet and a reversible hydrogen electrode were used as the counter electrode and reference electrode, respectively. For the preparation of the working electrodes, 8 mg of electrocatalyst powder was dispersed in 1 mL water and mixed for 30 minutes in an ultrasonic bath. Then, 20 μL of Nafion® solution (5%) was added, and the suspension was again mixed in an ultrasonic bath for 30 minutes. Five microlitre aliquots of the dispersion were pipetted onto the glassy carbon support surface and dried at 60 °C. The measurements were performed at 25 °C.

Before the CO stripping, cyclic voltammograms were performed in 0.5 mol L^{-1} H_2SO_4 purged with N_2 over a potential range from 0.05 to 1 V vs. a reversible hydrogen electrode (RHE) using a scan rate of 50 mV s^{-1} for electrocatalyst activation. Afterwards, the working electrode was polarized at 0.2 V while CO was purged for 5 minutes. Then, N_2 was purged for 25 minutes to remove the CO gas in the 0.5 mol L^{-1} H_2SO_4 solution. Further, three cycles were performed from 0.05 to 1 V at a scan rate of 10 mV s^{-1}. In the first one, the trial seeks CO oxidation, and through the others confirms the CO absence on the electrocatalyst surface.

The voltammetry for ethanol oxidation followed the same electrochemical conditions as CO stripping (0.05 to 1 V at a scan rate of 10 mV s^{-1}) but using 1.0 mol L^{-1} ethanol in 0.5 mol L^{-1} H_2SO_4 support electrolyte. Ethanol oxidation chronoamperometry was performed at 0.5 V for 1800 seconds. The results were compared with the commercial material Pt_3Sn_1/C E-TEK with a metal loading of 20% (w/w) supported on Vulcan® XC – 72 carbon because it is a reference material for ethanol oxidation reaction.

To monitor the formation of products during the ethanol electrochemical oxidation reaction, the in situ ATR-FTIR method of Silva et al.[22] was used. These measurements were performed using a Varian® IR 660 spectrometer equipped with a mercury cadmium telluride detector (MCT) that was cooled with liquid N_2 and an ATR crystal plate accessory with diamond/ZnSe. The experiments were performed at 25 °C under an N_2 atmosphere using a 1.0 mol L^{-1} ethanol solution in a 0.1 mol L^{-1} $HClO_4$ medium (to prevent the adsorption of sulphate). After the experiment, all the adsorption bands were deconvoluted into Lorentzian line forms. The normalized integrated intensities of the acetic acid, acetaldehyde and CO_2 bands are presented in this work, and the intensity and line width of each band was analysed individually.

3. Results and Discussion

3.1. Physicochemical Characterization

The chemical functionalization of the multiwalled carbon nanotubes with carboxylate groups and the changes after deposition of the metallic nanoparticles in the polymeric resin with subsequent heat treatment were observed by ATR-FTIR spectroscopy. In the spectra presented in Figure 1(a), the two peaks at 2925 cm^{-1} and 2848 cm^{-1}[23,24] corresponded to the vibrations of alkyl chain –CH.[25] The absorbance at 1633 cm^{-1}[25–27] was assigned to the C=O stretching of the –COOH group, and the peak at 1111 cm^{-1}[26] was attributed to C–O stretching vibrations. The functionalization process increased the hydrophilicity

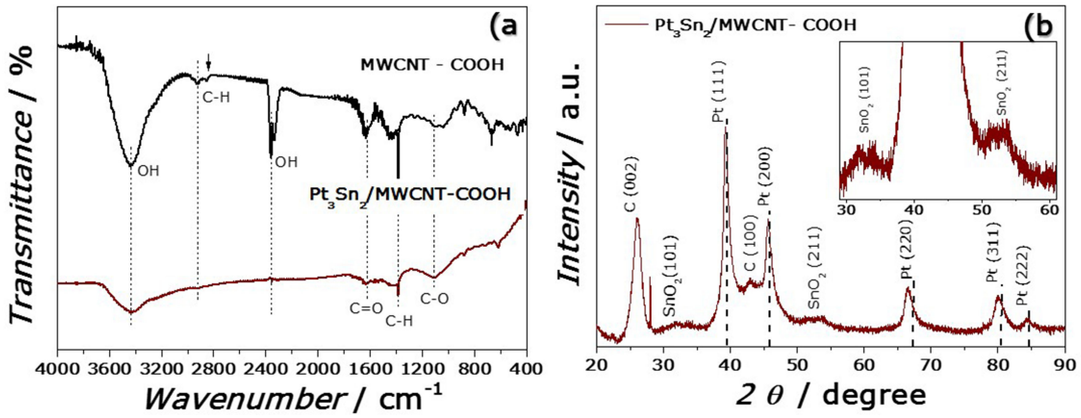

Figure 1. a) ATR-FTIR spectra of the pure functionalized support (MWCNT-COOH) and Pt_3Sn_2/MWCNT-COOH electrocatalyst. b) X-ray diffraction (XRD) pattern of the Pt_3Sn_2/MWCNT-COOH electrocatalyst prepared by the polymeric precursor method (dashed lines indicate the diffraction peaks from pure Pt).

due to the attack of functional groups containing oxygen, such as NO, on the CNT surface. This process yielded sites that anchored the metal nanoparticles. In addition, the CNT support had peaks at 3432 cm^{-1}[26-28] and 2362 cm^{-1} that corresponded to the hydroxyl group stretching vibration from carboxyl groups (O=C–OH and C–OH)[29] and the strongly hydrogen bonded –COOH.[29,30] These peaks indicated that carboxylic acid groups were formed on the surfaces of the MWCNTs. However, the thermal treatment and composite formation of the metal anchorage in the preparation method of the electrocatalyst can consume some of the functional groups, as observed in the Pt_3Sn_2/MWCNT-COOH spectra and by Arvand and Hassannezhad.[31]

The diffractogram of the Pt_3Sn_2/MWCNT-COOH electrocatalyst is presented in Figure 1(b). The diffraction peaks at 2 $\theta \approx 26.1^\circ$ and 42.7° were assigned to the (002) and (100) planes, respectively, of the graphitic hexagonal phase.[32] The peak sharpness of the (002) face indicates crystallinity was maintained in the Pt_3Sn_2/MWCNT-COOH after the COOH- functionalization process[33] and heat treatment in the electrocatalyst preparation. The X-ray diffractogram for the electrocatalyst showed peaks that were characteristic of the face-centred cubic crystalline structure of Pt (JCPDF #040802)[34] related to (111), (200), (220), (311) and (222) planes (Figure S1 – Support Information). However, the diffraction peaks shifted slightly to lower 2Θ angles with respect to pure Pt (dashed line in Figure 1(b)), likely due to the presence of Sn atoms, which can expand the Pt lattice parameter, allowing the formation of an alloy. Based on the Bragg equation for the Pt (220) plane, the lattice parameter obtained for the Pt_3Sn_2/MWCNT-COOH electrocatalyst was 0.3979 nm, and the mean crystallite size estimated by the Scherrer equation was approximately 4.65 nm.

These results indicate that the Sn was used in the synthesis process may be partially linked with Pt to form an alloy. Thus, the proportion of Sn in the alloy material was determined using the method described by Colmati et al.[35] for PtSn alloys. Overall, a Sn fraction of 0.32 was calculated, which corresponded to 32% Sn in the alloy form. The remaining fraction was most likely in the form of SnO_2 (cassiterite) due to the presence of discrete peaks at approximately 33° and 52°, which correspond to the (101) and (211) reflection planes of the SnO_2 (JCPDF #411445) phase observed in the X-ray diffractogram. Similar results were observed in others studies that used PtSn.[36–38]

The wettability of the electrocatalysts was analysed by contact angle measurements (Figure 2) over 10 minutes. The

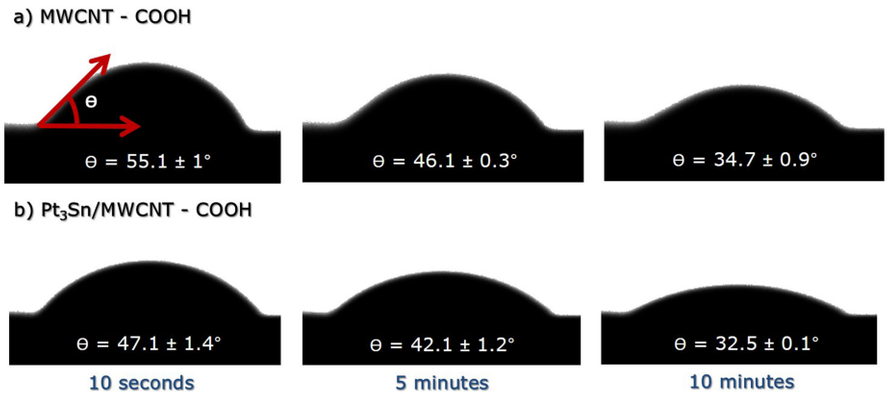

Figure 2. Contact angle images of water on a) MWCNT-COOH, b) Pt_3Sn_2/MWCNT-COOH at 1 min, 5 min and 10 min. $T = 20\,^\circ C$.

preparation method of the electrocatalysts (with the partial consumption of OH from functionalization, as observed in Figure 1(a)) slightly increased the hydrophilicity of the multiwalled carbon nanotubes. Additionally, SnO_2 species were formed on the electrocatalyts, as observed by XRD, which favoured surface hydration. The presence of oxygen in the electrocatalyst was also analysed by EDX (≈11%), while the pure support presented only about 4% of oxygen before the nanoparticle anchorage and thermal treatment, also seen by.[39]

Figure 3 shows the particle size distribution and the mean particle size. The electrocatalyst showed good polydispersity and size distribution on the carbon support. The particle sizes of the Pt_3Sn_2/MWCNT-COOH electrocatalyst were between 1 and 9 nm for 100% of the particles. The average estimated particle size was 3.85 ± 1.17 nm, which was within the range of experimental error of the value obtained from the Scherrer equation and the XRD measurements (4.65 nm). This difference, and the greater value obtained by XRD, resulted from the weak anchorage on the support, which favoured crystallite growth and/or the sintering process that occurred near 500°.[40] Additionally, the value obtained from the Scherrer equation was influenced by the experimental and structural factors that contributed to the width and are non-zero. However, similar results were obtained by Wang et al.[41] when using multiwalled carbon nanotubes functionalized with tetrahydrofuran as a support for PtSn electrocatalysts in the ethanol oxidation reaction.

For the MWCNT-COOH (Cheaptubes®), the oxidation treatment generates defects and introduces carboxyl groups (–COOH), hydroxyl (–OH) or carbonyl (–C=O) groups, onto MWCNT surface, increasing the attraction forces between metal-support, since these groups can anchor the precursors of noble metal ions by coordination or electrostatic interaction for nucleation, and subsequently reduction/deposition.[42,43] The surface acid oxygen groups are considered weak anchoring sites enhancing the dispersion of nanoparticles, while -Cπ (defects) and C=O groups acting as anchoring centers (strong interaction).[44]

The Pt precursor standard reduction potential is higher than the of Sn precursor one,[45] and probably there is a competition between metal-support and metal-metal interactions, because the delocalized p electrons of the MWCNT can be transferred to the metal, decreasing the Pt d-band vacancy (effect similar for Sn as an auxiliary metal).[46] Therefore, the unalloyed Sn can interact with oxygen surface due its strong affinity toward oxygen species (oxophilicity) to form SnO_2 weakly anchored.[47]

Hence, the formation of segregated phases in the electrocatalyst was due to the functionalization of the carbon nanotube support, which increased the affinity of Pt, facilitating interactions with the metal and interfering with the formation of the alloy. For untreated Vulcan XC 72 (used in this work), there is no specific anchoring sites on its surface, and then this mechanism for nanoparticle supporting was not considered, because the interaction between metal-metal is favored[45] and an electrocatalyst with 91–92% Sn alloyed with Pt was obtained when using this carbon support and the same preparation method.[8,21,22]

In addition to the HRTEM measurements, AFM was used to obtain three-dimensional images of the surface morphology and information about the roughness. The images are shown in Figure 4. The AFM measurements were used to determine the root mean square of the roughness (Rq) of the MWCNT-COOH and the Pt_3Sn_2/MWCNT-COOH, which was 0.2855 ± 0.066 μm and 0.1671 ± 0.009 μm, respectively. The decrease in roughness of the supported nanoparticles relative to the pure support can be attributed to the thermal treatment (400 °C) (sintering/calcination process) during the preparation. This effect was also observed by Yu et al.[48] for a bare ITO surface, which became smooth after silver ion implantation to produce an AgNP/ITO electrode. The nanotube functionalization generates defects on the structure, which provide more sites for anchoring. Therefore, the roughness and surface energy (they tend to agglomerate) are higher than for nanoparticles/MWCNT-COOH. During the thermal treatment, the particles anchorage fills the defects and the calcination can forms a new interface, decreasing the roughness.

The AFM results indicate a morphological change as a result of the metallic nanoparticle anchorage process for Pt_3Sn_2/MWCNT-COOH compared to Pt_3Sn_1/C E-TEK. Furthermore, the root mean square roughness (Rq) of Pt_3Sn_1/C E-TEK is lower

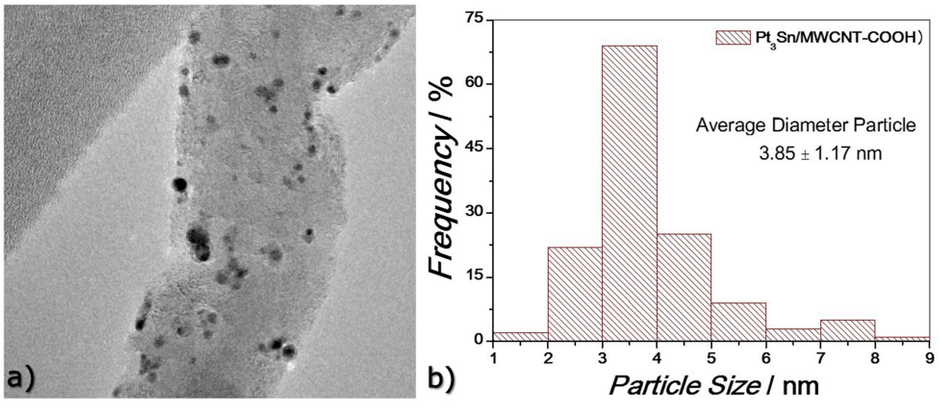

Figure 3. a) Pt_3Sn_2/MWCNT-COOH electrocatalyst TEM image and b) histogram showing the particle size distribution of the electrocatalyst.

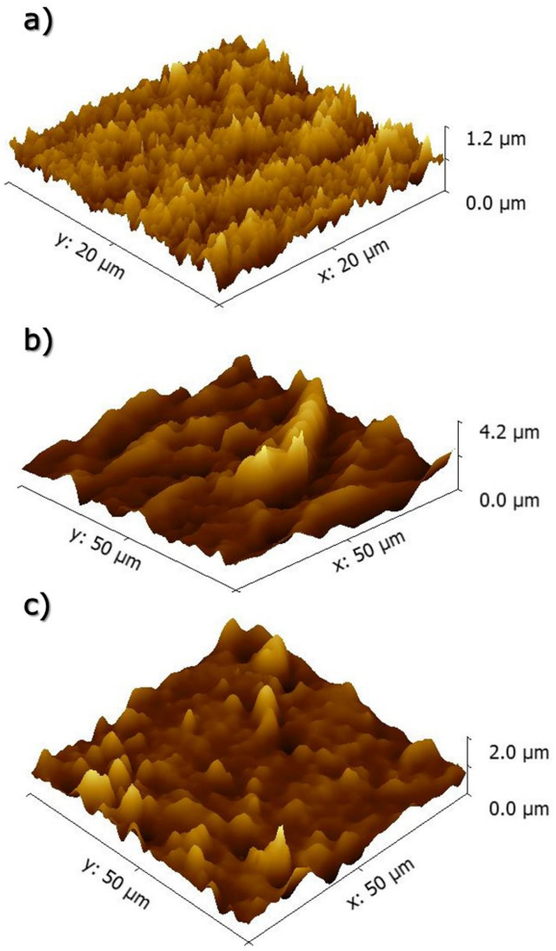

Figure 4. AFM three-dimensional (3D) images of a) Pt_3Sn_1/C E-TEK, b) MWCNT-COOH, and c) Pt_3Sn_2/MWCNT-COOH..

(0.1318 ± 0.009 µm) than that of Pt_3Sn_2/MWCNT-COOH 0.1671 ± 0.009 µm. Although these values are not indicative of the electrochemical active surface area (EASA), they are in agreement with the other values obtained.

3.2. Electrochemical Activity Measurements

Figure 5 shows that Pt_3Sn_2/MWCNT-COOH has slightly lower oxidation onset potential for CO than Pt_3Sn_1/C E-TEK (0.32 V and 0.39 V, respectively). Both materials present oxidation peaks centred at 0.8 V, but the normalized current peak on the Pt_3Sn_2/MWCNT-COOH electrocatalyst is 3.5 times greater than on Pt_3Sn_1/C E-TEK for the same process. The Pt particle size influences the CO oxidation peak potential.[49] According to the literature the CO oxidation peak shift to lower overpotential as the nanoparticles size increases.[41,50,51] Thus, both materials present a peak CO oxidation potential close to 0.8 V, indicating that there is no a huge difference in the particle size. Pt_3Sn_1/C E-TEK has a particle size of approximately 3.8–4 nm[52,53] (as confirmed in Figure S2 in Support Information), and the material prepared from the polymeric precursor has a particles size of 3.85 nm, as observed in the HRTEM analysis. However, a shoulder is observed at approximately 0.64 V for the CO oxidation on the material supported on carbon nanotubes. Since there is a similar particle size for both materials, other factors, such as the metal composition and carbonaceous supports, should be considered. Pt_3Sn_2/MWCNT-COOH has a mass ratio of 3:1 (atomic ratio 3:2), as measured by EDS, while Pt_3Sn_1/C E-TEK has an atomic ratio of 3:1 (mass ratio 9:1). Thus, the material supported on carbon nanotubes has a greater Sn content than the commercial material. Moreover, the polymeric precursor method produced a electrocatalyst with only 32% alloy formation on the carbon nanotubes, while Pt_3Sn/C E-TEK electrocatalysts have a percentage greater than 60%.[52,53] The literature discusses two pathways for CO oxidation on PtSn electrocatalysts: (i) a bifunctional mechanism, in which CO adsorption occurs only on Pt and OH interacts preferentially with the adsorbed Sn,[54] which promotes water dissociation and CO oxidation simultaneously at potentials lower than on Pt[55] and (ii) an electronic effect in alloy surfaces where the second metal alters the Pt electronic properties and weakens the CO adsorption strength, limiting CO poisoning on the surface and becoming more active for the reaction.[56]

In this study, the presence of Sn (alloy phase) and SnO_2 (segregated phase) on the surface of the electrocatalyst prepared by the polymeric precursor method has a synergic effect that is more effective than the commercial material. Oxide species can inhibit the Pt sites and decrease the CO accessibility to the Pt sites, generating various surface sites with different CO adsorption[57] energy and broadening the peak. Hence, a shoulder appears at 0.64 V for the material supported on MWCNTs, and the CO oxidation onset potential is shifted. Baranova et al.[58] studied alloy and bi-phase PtSn/C electrocatalysts prepared by the polyol method for the ethanol oxidation reaction in alkaline medium and observed the shoulder for CO oxidation in some materials. They obtained better results using bi-phase electrocatalysts than alloy materials.

The influence of the support has also been considered on the electrocatalyst properties. Based on a previous work,[8,21,22] the polymeric precursor preparation method was used to produce a Pt_3Sn electrocatalyst supported on Vulcan® carbon, and the Pt_3Sn alloy formation was 91–92%. In this work, the same preparation method was used, but the obtained electrocatalyst had only 32% alloy phase. Multiwalled carbon nanotubes functionalized with –COOH groups promoted metallic nanoparticle anchorage, mainly Pt, and favoured segregated SnO_2 species formation, providing oxygen species that assisted in the oxidation of CO.[59] Moreover, the presence of tin oxide on the surface of the electrocatalyst can help to oxidize CO through bifunctional mechanisms.[35,60] Simultaneously, the partial formation of Pt_3Sn alloy on MWCNTs may change the electronic structure of Pt and weaken the CO adsorption on the surface[13] at low potential, while on the commercial material with high alloying degree, CO_{ads} oxidation was observed in a narrow potential range. These effects can explain the difference in the electrocatalytic activity for ethanol oxidation using Pt_3

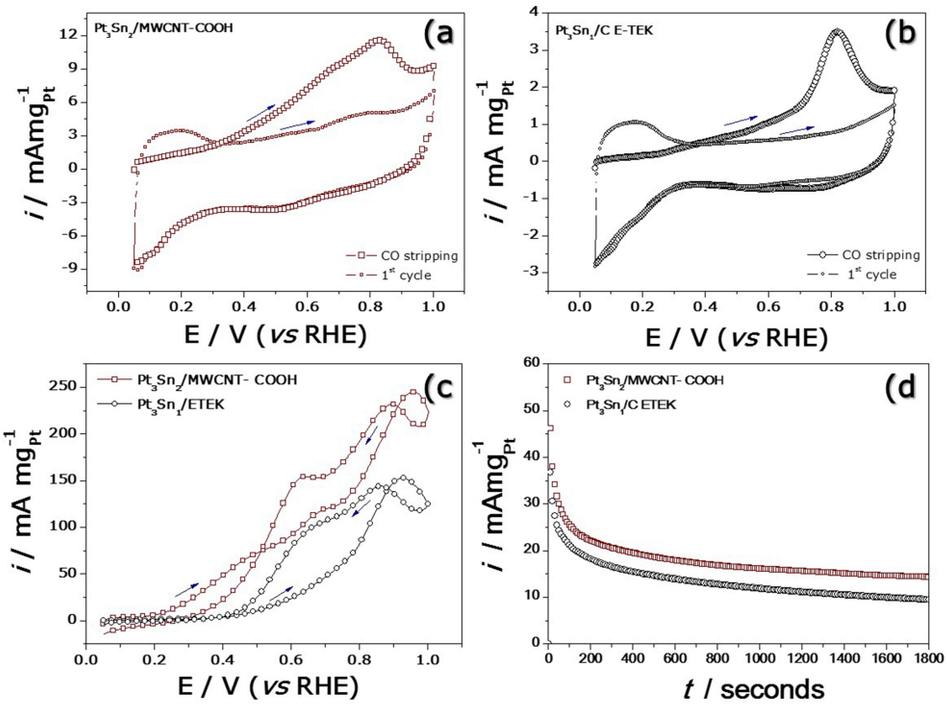

Figure 5. Cyclic voltammograms for CO stripping ($v = 10\ mV\,s^{-1}$) using a) Pt_3Sn_2/MWCNT-COOH and b) Pt_3Sn_1/C E-TEK. c) Cyclic voltammograms ($V = 10\ mV\,s^{-1}$) and b) chronoamperometry at 0.5 V for 1800 sec for ethanol oxidation ($1.0\ mol\,L^{-1}$) in $0.5\ mol\,L^{-1}\ H_2SO_4$. $T = 25\,^{\circ}C$.

Sn_2/MWCNT-COOH electrocatalyst compared to the commercial material.

From the first voltammetric cycle to after CO oxidation, for both materials, the hydrogen desorption region is not well defined (0.05 V–0.4 V vs. RHE) due to alloy formation between Pt and Sn.[61] Assuming a clean surface, cyclic voltammetry was used to estimate the electrochemical active surface area (EASA), with $210\ \mu C\,cm^{-2}$ as the desorption charge for hydrogen (UPD) on Pt[62] and an electrode loading ($mg\,Pt\,cm^{-2}$) that is the Pt mass per unit area of the electrode ($0.11\ cm^2$). The EASA of Pt_3Sn_2/MWCNT-COOH and Pt_3Sn_1/C E-TEK was $88.75\ cm^2\,mg_{Pt}^{-1}$ and $42.73\ cm^2\,mg_{Pt}^{-1}$, respectively. Even though Pt_3Sn_1/C (75:25) E-TEK has more Pt in the bulk compared to Pt_3Sn_2/MWCNT-COOH (64:36), the electrochemical surface area of the latter is more than two times greater.

The onset potential for ethanol oxidation, shown in Figure 5(c), using the Pt_3Sn_2/MWCNT-COOH electrocatalyst was 0.21 V less positive than that obtained by the commercial Pt_3Sn_1/C E-TEK. Furthermore, the normalized current peak for the ethanol oxidation reaction using the Pt_3Sn_2/MWCNT-COOH electrocatalyst was $250\ mAmg_{Pt}^{-1}$, while that of the commercial material for the same process was $150\ mAmg_{Pt}^{-1}$. The material supported on MWCNT-COOH has both a PtSn alloy phase and SnO_2 species. The Sn alloy with the Pt electrocatalyst decreased the intensity of CO adsorption while SnO_2 provided OH_{ads} on the surface of the electrocatalyst, which assisted in the ethanol oxidation at lower potentials than on Pt. In the alloy phase the close contact between the elements of different work functions promotes charge transport from one metal to another until the Fermi level of electrons at the interface is equilibrated, this phenomena is called electronic effect, this phenomenon weakens the bond strength of the poisoning species on the catalyst surface, which is well known as electronic effect.[58,63] On the other hand, SnO_2 plays an important role providing OH at lower overpotential than platinum, favoring the oxidation of intermediate species, which is well known as bifunctional effect.[22,63] Thus, the shift of the ethanol electro-oxidation onset potential, using electrocatalysts containing to phases (PtSn alloy and SnO_2), suggests the synergic effect of the two phenomena, knowing as bifunctional effect and electronic effect, improving the materials electrocatalytic activity for ethanol electro-oxidation.[58,63] Considering these features and hat the EASA from Pt_3Sn_2/MWCNT-COOH was higher than that of Pt_3Sn_1/C E-TEK, the superior electroactivity obtained by the prepared material is justified.

The studies presented in Figure 6 are: (a) the material electrocatalytic activities for the oxidation of ethanol under potentiostatic conditions (0.5 V for 1800 seconds), (b) monitoring of the formation of products in the potential region between 0.2 and 1 V using in situ ATR-FTIR, and (c) the intensity bands of the products formed depending on the potential (in the in situ FTIR spectrum) of ethanol oxidation with the Pt_3Sn_2/MWCNT-COOH electrocatalyst.

Pt_3Sn_2/MWCNT-COOH electrocatalyst showed a greater current density for ethanol oxidation ($16\ mA\,mg_{Pt}^{-1}$) after 1800 seconds than that of the commercial electrocatalyst ($10\ mA\,mg_{Pt}^{-1}$), in Figure 5d. The material supported on CNTs favoured acetaldehyde production (see Figure 6b). Carboxyl

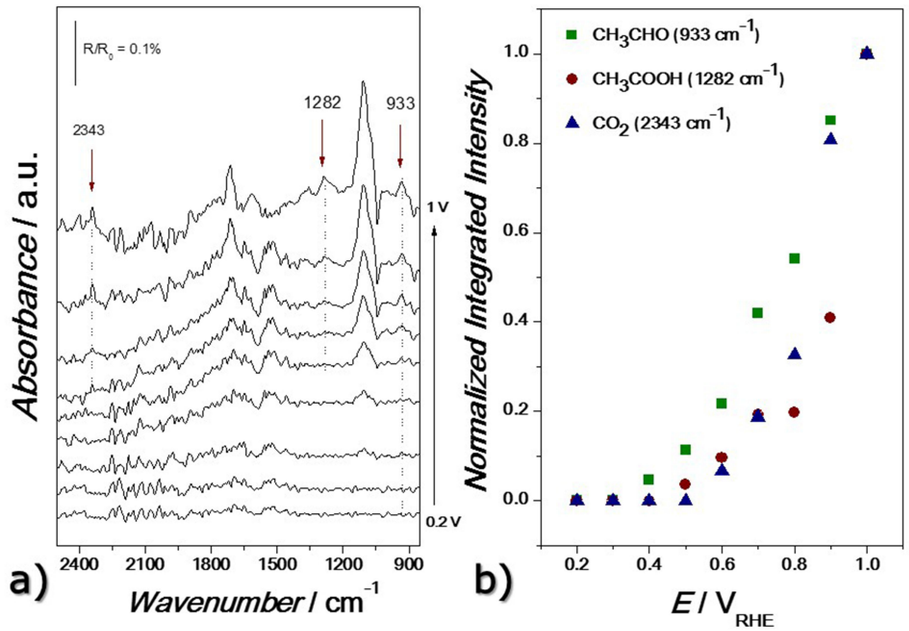

Figure 6. a) The in situ FTIR spectra collected at several potentials (0.2 to 1 V) for ethanol (1.0 mol L^{-1}) oxidation in 0.1 mol L^{-1} $HClO_4$ (with the background collected at 0.05 V/RHE); and b) integrated acetaldehyde (933 cm^{-1}), acetic acid (1282 cm^{-1}) and carbon dioxide (2343 cm^{-1}) IR band intensities as a function of the electrode potential on the Pt_3Sn_2/MWCNT-COOH electrocatalyst.

groups can form hydrogen bonds with water molecules to improve the dissociation process of the molecules during the ethanol oxidation reaction.[64] The presence of oxygen functional groups at the edges and on the surface of the CNTs functionalized by acid treatment[49] favours interactions between the substrate and the metallic alloy[65] and contributes to the stability of the electrocatalyst, keeping the normalized current for the EOR higher than when using Pt_3Sn_1/C E-TEK.

The products generated during the ethanol oxidation reaction were measured by in situ ATR-FTIR, and the results are shown in Figure 6. Absorbance bands related to acetaldehyde (933 cm^{-1}),[66] acetic acid (1282 cm^{-1})[67] and CO_2 (2343 cm^{-1})[68] were observed. Additionally, peaks 1050 cm^{-1}, 1130 cm^{-1} and 1715 cm^{-1} were assigned to ν_a (CCO) from the ethanol consumption band, perchloride ion adsorption and C=O stretching of the carbonyl groups from acetic acid and acetaldehyde.[69] When using Pt_3Sn_2/MWCNT-COOH, acetaldehyde is observed at 0.2 V vs. RHE and 0.3 V for Pt_3Sn_1/C E-TEK, as observed by Souza et al.[70] under the same conditions. Acetaldehyde is the majority product formed during the EOR at all potentials. Acetic acid and CO_2 were observed at 0.4 V and 0.6 V, respectively. In order to make the signals visible we have zoomed out the regions corresponding to CO_2, acetic acid and acetaldehyde as can be seen in the Figure S3 (a), (b) and (c), respectively.

Acetaldehyde is produced at lower potentials because the reaction requires less energy, while acetic acid and CO_2 production occurs at high potentials because it requires higher energies. However, it is not possible to confirm that acetic acid and CO_2 are direct products of acetaldehyde.[68] Pt_3Sn_1/C E-TEK[70] had higher acetic acid formation than acetaldehyde and CO_2 because the Pt_3Sn alloy phase in this material (greater than 60%) increased the Pt–Pt distance and inhibited the C–H bonds dissociation of the ethanol molecule, producing acetic acid instead of CO_2. Considering the superior EASA, the lower potential and higher normalized current for the EOR and the possibility to produce CO_2 at approximately 0.6 V, the Pt_3Sn_2/MWCNT-COOH is a promising electrocatalyst for this reaction.

4. Conclusions

The use of MWCNT-COOH affects the morphology and structure of the electrocatalyst, favouring SnO_2 formation segregated with Pt (68%) compared to 32% in the Pt_3Sn/C alloy formation. Previous work[8,21,22] achieved 91–92% Pt_3Sn alloy on Vulcan® carbon using the same preparation method. The Pt_3Sn_2/MWCNT-COOH had larger EASA, lower onset potential and higher normalized peak current for the EOR. Additionally, the material supported on MWCNT-COOH presented a pathway for EOR that preferred acetaldehyde at low potentials and acetic acid/CO_2 at potentials greater than 0.5 V, while Pt_3Sn_1/C E-TEK favoured acetic acid production. Thus, MWCNTs are promising supports for the oxidation of ethanol in direct ethanol fuel cells based on their electroactive surface area, chemical composition and stability.

Acknowledgements

The authors are grateful to the Central Experimental Multiusuário UFABC, Laboratório de Nanocaracterização da UFSCAR and

Fapesp (Process Numbers 2011/00008-2, 2013/01577-0 and 2015/10314-8), CNPq (150532/2016-4 and 406612/2013-7).

Conflict of Interest

The authors declare no conflict of interest.

[1] J. M. Andújar, F. Segura, *Renew. and Sustain. Energ. Rev.* **2009**, *13 (9)*, 2309–2322.
[2] M. A. F. Akhairi, S. K. Kamarudin, *Int. J. Hydrogen Energy* **2016**, *41*, 4214–4228.
[3] D. H. Lim, D. H. Choi, W. D. Lee, H. I. Lee, *Appl. Catal. B* **2009**, *89 (3-4)*, 484–493.
[4] S. C. Zignani, V. Baglio, J. J. Linares, G. Monforte, E. R. Gonzalez, A S Aricó, *Electrochim. Acta* **2012**, *70*, 255–265.
[5] E. Antolini, E. R. Gonzalez, *Catal. Today* **2011**, *160*, 28–38.
[6] L. Li, M. Huang, J. Liu, Y. Guo, *J. Power Sources* **2011**, *196*, 1090–1096.
[7] J. Asgardi, J. C. Calderón, F. Alcaide, A. Querejeta, L. Calvillo, M. J. Lázaro, G. García, E. Pastor, *Appl. Catal. B* **2015**, *168–169*, 33–38.
[8] R. F. B. Souza, L. S. Parreira, D. C. Rascio, J. C. M. Silva, E. Teixeira-Neto, M. L. Calegaro, E. V. Spinacé, A. O. Neto, M. C. Santos, *J. Power Sources* **2009**, *195*, 1589–1593.
[9] L. Jiang, Z. Zhou, W. Li, W. Zhou, S. Song, H. Li, G. Sun, Q. Xin, *Energy Fuels* **2004**, *18*, 866–871.
[10] M. Zhu, G. Sun, Q. Xin, *Electrochim. Acta* **2009**, *54*, 1511–1518.
[11] D. R. M. Godoi, J. Perez, H. M. Villullas, *J. Power Sources* **2010**, *195*, 3394–3401.
[12] K. S. Lee, I. S. Park, Y. H. Cho, D. S. Jung, N. Jung, H. Y. Park, Y. E. Sung, *J. Catal.* **2008**, *258*, 143–152.
[13] J. E. Thomas, A. R. Bonesi, M. S. Moreno, A. Visintin, A. M. Castro Luna, W. E. Triaca, *Int. J. Hydrogen Energy* **2010**, *35*, 11681–11686.
[14] C. Wang, H. Li, J. Zhao, Y. Zhu, W. Z. Yuan, Y. Zhang, *Int. J. Hydrogen Energy* **2013**, *38 (30)*, 13230–13237.
[15] J. M. Sieben, M. M. E. Duarte, *Int. J. Hydrogen Energy* **2011**, *36*, 3313–3321.
[16] D. Chu, Z. Li, X. Yuan, J. Li, X . Wei, Y. Wang, *Electrochim. Acta* **2012**, 78, 644–657.
[17] A. N. Geraldes, D. F. Silva, J. C. M. Silva, O. A. Sá, E. V. Spinace, A. O. Neto, M. C. Santos, *J. Power Sources* **2015**, 275, 189–199.
[18] P. Hernández-Fernández, M. Montiel, P. Ocón, J. L. Gómez de la Fuente, S. García-Rodríguez, S. Rojas, J. L. G. Fierro, *Appl. Catal. B* **2010**, *99 (1–2)*, 343–352.
[19] S. Sharma, B. G. Pollet, *J. Power Sources* **2012**, *208*, 96–119.
[20] C. Yang, D. Wang, X. Hu, C. Daia, L. Zhang, *J. Alloys Compd.* **2008**, *448 (1–2)*, 109–115.
[21] A. Amorim, L. S. Parreira, J. C. M. Silva, M. C. Santos, *J. Braz. Chem. Soc.* **2016**, *00*, 1–7.
[22] J. C. M. Silva, L. S. Parreira, R. F. B. Souza, M. L. Calegaro, E. V. Spinacé, A. O. Neto, M. C. Santos, *Appl. Catal. B* **2011**, *110 (2)*, 141–147.
[23] B. Zhang, Q. Chen, H. Tang, Q. Xie, M. Ma, L. Tan, Y. Zhang, S. Yao, *Colloids Surf. B* **2010**, *80 (1)*, 18–25.
[24] G. Fang, W. Gao, Q. Deng, K. Qian, H. Han, S. Wang, *Anal. Biochem.* **2012**, *423 (2)*, 210–217.
[25] L. Liu, H. D. Wagner, *Composit. Sci. Tech.* **2005**, *65 (11–12)*, 1861–1868.
[26] Q. Wang, L. Zhou, Y. Jiang, J. Gao, *Enzyme Microb. Technol.* **2011**, *49 (1)*, 11–16.
[27] H. Zarei, H. Ghourchian, K. Eskandari, M. Zeinali, *Anal. Biochem.* **2012**, *421 (2)*, 446–453.
[28] C. Zhou, S. Wang, Q. Zhuang, Z. Han, *Carbon* **2008**, *46 (9)*, 1232–1240.
[29] P. Gupta, S. Sharan, P. Roya, D. Lahiria. *Carbon* **2015**, *95*, 715–724.
[30] R. E. C. Torrejos, G. M. Nisola, M. J. Park, H. K. Shon, J. G. Seo, S. Koo, W. J. Chung, *Chem. Eng. J.* **2015**, *264*, 89–98.
[31] M. Arvand, M. Hassannezhad, *Mater. Sci. Eng. C* **2014**, *36*, 160–167.
[32] Y. C. Chiang, W. H. Lin, Y. C. Chang, *Appl. Surf. Sci.* **2011**, *257*, 2401–2410.
[33] T. A. Saleh, *Appl. Surf. Sci.*, **2011**, *257*, 7746–7751.
[34] J. Haglund, F. Fernandez Guillermet, G. Grimvall, M. Korling, *Phys. Rev. B: Condens. Matter Mater. Phys.* (18, 1978-) **1993**, *48*, 11685–11691.
[35] F. Colmati, E. Antolini, E. R. Gonzalez, *J. Electrochem. Soc.* **2007**, *154*, B39-B47.
[36] R. M. Antoniassi, A. O. Neto, M. Linardi, E. V. Spinacé, *Int. J. Hydrogen Energy* **2013**, *38 (27)*, 12069–12077.
[37] D. H. Lim, D. H. Choi, W. D. Lee, H. I. Lee, *Appl. Catal. B* **2009**, *89 (3–4)*, 484–493.
[38] L. Jiang, L. Colmenares, Z. Jusys, G. Q. Sun, R. J. Behm, *Electrochim. Acta* **2007**, *53 (2)*, 377–389.
[39] M. Kah, X. Zhang, T. Hofmann, *Sci. Total Environ.* **2014**, *497–498*, 133−138.
[40] F. Colmati, E. Antolini, E. R. Gonzalez, *Appl. Catal. B* **2007**, *73 (1–2)*, 106–115.
[41] D. Wang, S. Lu, S. P. Jiang. *Electrochim. Acta* **2010**, *55 (8)*, 2964–2971.
[42] B. Wu, D. Hu, Y. Kuang, Y. Yu, X. Zhang, J. Chen, *Chem. Commun.* **2011**, 47, 5253–5255.
[43] S. Shahgaldi, J. Hamelin, *Carbon* **2015**, *94*, 705–728.
[44] X. Yu, S. Ye, *J. Power Sources* **2007**, *172*, 33–144.
[45] L. Jiang, G. Sun, Z. Zhou, W. Zhou, Q. Xin, *Catal. Today* **2004**, *93–95*, 665–670.
[46] S. Zhang, Y. Shao, G. Yina, Y. Lin, *J. Mater. Chem. A* **2013**, *1*, 4631–4641.
[47] S. M. Choi, M. H. Seo, H. J. Kim, W. B. Kim, *Synth. Met.* **2011**, *161*, 2405–2411.
[48] Y. Yu, M. Jia, H. Tian, J. Hu, *J. Power Sources* **2014**, *267*, 123–127.
[49] L. Calvillo, V. Celorrio, R. Moliner, A. B. Garcia, I. Caméan, M. J. Lazaro, *Electrochim. Acta* **2013**, *102*, 19–27.
[50] O. V. Cherstiouk, P. A. Simonov, E. R. Savinova, *Electrochim. Acta* **2003**, *48*, 3851–3860.
[51] A. Cuesta, A. Couto, A. Rincón, M. C. Pérez, A. López-Cudero, C. Gutiérrez , *J. Electroanal. Chem.* **2006**, *586*, 184–195.
[52] L. Colmenares, H. Wang, Z. Jusys, L. Jiang, S. Yan, G. Q. Sun, R. J. Behm. *Electrochim. Acta* **2006**, *52*, 221–233.
[53] F. Colmati, E. Antolini, E. R. Gonzalez, *J. Power Sources* **2006**, *157*, 98–103.
[54] W. D. Michalak, J. M. Krier, S. Alayoglu, J. Y. Shin, K. An, K. Komvopoulos, Z. Liu, G. A. Somorjai, *J. Catal.* **2014**, *312*, 17–25.
[55] C. Dupont, Y. Jugnet, D. Loffreda, *J. Am. Chem. Soc.* **2006**, *128*, 9129–9136.
[56] A. Sümer, A. E. Aksoylu, *Surf. Sci.* **2008**, *602*, 1636–1642.
[57] E. M. Crabb, R. Marshall, D. Thompsett, *J. Electrochem. Soc.* **2000**, *147 (12)*, 4440–4447.
[58] E. A. Baranova, M. A. Padilla, B. Halevi, T. Amir, K. Artyushkova, P. Atanassov, *Electrochim. Acta* **2012**, *80*, 377–382.
[59] M. Carmo, V. A. Paganin, J. M. Rosolen, E. R. Gonzalez, *J. Power Sources* **2005**, *142*, 169–176.
[60] M. Arenz, V. Stamenkovic, B. B. Blizanac, K. J. J. Mayrhofer, N. M. Markovic, P. N. Ross, *J. Catal.* **2005**, *232 (2)*, 402–410.
[61] D.-H. Lim, D.-H. Choi, W.-D. Lee, H.-I. Lee, *Appl. Catal. B* **2009**, *89*, 484–493.
[62] M. Watanabe, H. Sei, P. Stonehart, *J. Electroanal. Chem.* **1989**, *261*, 375–387.
[63] T. L. Lomocso, E. A. Baranova, *Electrochim. Acta* **2011**, *56*, 8551–8558.
[64] L. Q. Hoa, M. C. Vestergaard, H. Yoshikawa, M. Saito, E. Tamiya, *Electrochem. Communic.* **2011**, *13*, 746–749.
[65] D. Chu, Z. Li, X. Yuan, J. Li, X. Wei, Y. Wan, *Electrochim. Acta* **2012**, *78*, 644–657.
[66] M. Li, A. Kowal, K. Sasaki, N. Marinkovic, D. Su, E. Korach, P. Liu, R. R. Adzic, *Electrochim. Acta* **2010**, *55*, 4331–4338.
[67] R. F. B. Souza, L. S. Parreira, D. C. Rascio, J. C. M. Silva, E. Teixeira-Neto, M. L. Calegaro, E. V. Spinace, A. O. Neto, M . C. Santos , *J. Power Sources* **2010**, *195*, 1589–1593.
[68] G.A. Camara, T. Iwasita, *J. Electroanal. Chem.* **2005**, *578*, 315–321.
[69] E. L. Silva, A. Cuña, M. R. O. Vega, C. Radtkec, G. Machado, N. Tancredi, C. F. Malfatti, *Appl. Catal. B* **2016**, *193,* 170–179.
[70] R. F. B. Souza, J. C. M. Silva, M. H. M. T. Assumpção, A. O. Neto, M. C. Santos, *Int. J. Hydrogen Energy* **2011**, *36 (18)*, 11519–11527.

Manuscript received: March 30, 2017
Accepted Article published: April 13, 2017
Version of record online: May 11, 2017